Mitophagy induction improves salivary gland stem/progenitor cell function by reducing senescence after irradiation

Cinat, Davide; Souza, Anna Lena De; Soto-Gamez, Abel; Jellema-de Bruin, Anne L; Coppes, Rob P; Barazzuol, Lara

Published in:
Radiotherapy and Oncology

DOI:
10.1016/j.radonc.2023.110028

Publication date:
2024

Radiotherapy and Oncology 190 (2024) 110028

Contents lists available at ScienceDirect

Radiotherapy and Oncology

journal homepage: www.thegreenjournal.com

Original Article

Mitophagy induction improves salivary gland stem/progenitor cell function by reducing senescence after irradiation

Davide Cinat [a,b], Anna Lena De Souza [a,b,1], Abel Soto-Gamez [a,b,1], Anne L. Jellema-de Bruin [a,b], Rob P. Coppes [a,b], Lara Barazzuol [a,b,*]

[a] Department of Biomedical Sciences of Cells & Systems, Section of Molecular Cell Biology, University Medical Center Groningen, University of Groningen, Groningen, the Netherlands
[b] Department of Radiation Oncology, University Medical Center Groningen, University of Groningen, Groningen, the Netherlands

ARTICLE INFO

Keywords:
Salivary glands
Irradiation
Senescence
Mitochondria
Stem cells

ABSTRACT

Background and purpose: Patients undergoing radiotherapy for head and neck cancer often experience a decline in their quality of life due to the co-irradiation of salivary glands. Radiation-induced cellular senescence is a key factor contributing to salivary gland dysfunction. Interestingly, mitochondrial dysfunction and cellular senescence have been reported to be strongly interconnected and thus implicated in several aging-related diseases. This study aims to investigate the role of mitochondrial dysfunction in senescence induction in salivary gland stem/progenitor cells after irradiation.

Materials and methods: A dose of 7 Gy photons was used to irradiate mouse salivary gland organoids. Senescent markers and mitochondrial function were assessed using rt-qPCR, western blot analysis, SA-β-Gal staining and flow cytometry analysis. Mitochondrial dynamics-related proteins were detected by western blot analysis while Mdivi-1 and MFI8 were used to modulate the mitochondrial fission process. To induce mitophagy, organoids were treated with Urolithin A and PMI and subsequently stem/progenitor cell self-renewal capacity was assessed as organoid forming efficiency.

Results: Irradiation led to increased senescence and accumulation of dysfunctional mitochondria. This was accompanied by a strong downregulation of mitochondrial fission-related proteins and mitophagy-related genes. After irradiation, treatment with the mitophagy inducer Urolithin A attenuated the senescent phenotype and improved organoid growth and stem/progenitor cell self-renewal capacity.

Conclusion: This study shows the important interplay between senescence and mitochondrial dysfunction after irradiation. Importantly, activation of mitophagy improved salivary gland stem/progenitor cell function thereby providing a novel therapeutic strategy to restore the regenerative capacity of salivary glands following irradiation.

Introduction

Head and neck cancer (HNC) is the seventh most prevalent cancer worldwide [1]. The primary treatment approach for the majority of HNC patients involves radiotherapy, often in conjunction with surgery and chemotherapy [1]. Unfortunately, radiotherapy leads to a decline in a patient's quality of life, primarily due to radiation-induced damage of normal tissues [2]. Xerostomia, or dry mouth syndrome, is a side effect that results from the co-irradiation of healthy salivary glands [3]. Consequently, patients suffer from impaired speech, dental issues, and difficulties with swallowing and speaking [3]. Understanding the precise mechanisms responsible for the long-term impairment of salivary gland function after irradiation remains limited.

Radiation-induced cellular senescence is a contributing factor of salivary gland dysfunction [4]. Studies have shown that senescence, especially in the salivary gland stem/progenitor cell niche, can result in impaired tissue regeneration and radiation-induced hyposalivation [5,6]. Cellular senescence can be triggered by various stressors and is characterized by a stable cell cycle arrest, resistance to apoptosis and secretion of senescent-associated secretory phenotype (SASP) factors

* Corresponding author.
E-mail address: l.barazzuol@umcg.nl (L. Barazzuol).
[1] These authors contributed equally.

https://doi.org/10.1016/j.radonc.2023.110028
Received 15 June 2023; Received in revised form 15 November 2023; Accepted 19 November 2023
Available online 24 November 2023

[7]. Mitochondrial dysfunction and cellular senescence have been shown to be strongly interconnected [8]. Indeed, the accumulation of dysfunctional mitochondria is typically accompanied by disrupted bioenergetics and increased production of reactive oxygen species (ROS), which contributes to the enforcement of the senescent phenotype [8]. Moreover, recent studies have shown a strong correlation between dysregulated mitochondria and the inflammatory microenvironment in the salivary gland of Sjogren's and aged patients [9,10].

Mitochondria are dynamic organelles, able to adapt to different energy requirements and stress conditions [11,12]. They organize as complex networks and their architecture constantly changes through fission and fusion processes, which are regulated by specific GTPases, such as Drp1, Mfn1, Mfn2 and Opa1 [11,13]. The disruption in the balance of this dynamic process has been shown to be implicated in inflammatory and aging-related diseases [8,14]. Furthermore, alterations in mitochondrial dynamics can profoundly influence stem cell function and self-renewal, contributing to loss in tissue regeneration capacity and a decline in organ function [15]. Through mitophagy, a highly selective autophagy process, cells can eliminate damaged mitochondria, re-establishing cellular homeostasis [16]. Importantly, defective mitophagy has been shown to affect the regenerative capacity of stem/progenitor cells in different tissues, contributing to their exhaustion and the onset of various aging-related disorders [17]. The effect of radiation on mitochondrial function and its causal role in the development of senescence in the response of salivary glands remain to be elucidated.

In this study, using mouse salivary gland organoids (mSGOs) that resemble the corresponding *in vivo* tissue and contain adult stem/progenitor cells [18], we show that radiation-induced senescence is associated with an accumulation of dysfunctional mitochondria due to impaired mitochondrial dynamics and reduced mitophagy. Rescue of mitophagy by using the mitophagy inducer agent, Urolithin A (UA), attenuated senescence and improved organoid growth and stem/progenitor cell function, revealing a promising new approach to ameliorate radiation-induced damage in the salivary gland and possibly other normal tissues.

Materials and methods

Mice

8-to 12-week-old female C57BL/6 mice (Envigo, the Netherlands) were housed under conventional conditions with a standard diet and water *ad libitum* at the central animal facility of the University Medical Center Groningen. Animal experimental procedures were approved by the Central Committee of Animal Experimentation of the Dutch government [license number AVD1050020184824] and the Institute Animal Welfare Body of the University Medical Center Groningen [animal welfare body (IVD) protocol number 184824–01-001].

Organoid culture and self-renewal assay

Submandibular glands were collected from adult female mice and isolated as previously described [19]. In brief, following mechanic and enzymatic digestion, cells were cultured in DMEM/F12 (Gibco/Invitrogen, cat#11320–074) supplemented with penicillin-streptomycin antibiotics (Invitrogen, cat#15140–163), glutamax (2 mM; ThermoFisher Scientific, cat#35050038), EGF (20 ng/ml; Sigma-Aldrich, cat#E9644); FGF2 (20 ng/ml; Peprotech, cat#100–18-B), N2 (1x; Gibco, cat#17502–048), insulin (10 μg/ml, Sigma-Aldrich, cat#I6634-100MG) and dexamethasone (1 uM; Sigma-Aldrich, cat#d4902-25 mg). After 3 days, primary spheres were dissociated into single cells using 0.05 % trypsin EDTA (Invitrogen, cat#25300–096). After counting, 10.000 cells were plated in 75 μL gel/well [35 μL cell suspension + 40 μL of culturex basement membrane extract Type 2 (BME) (R&D systems, cat#3532–010-02P)] in a 12-well tissue culture plate. After solidification of the gels, 1 mL of WRY medium [DMEM/F12, penicillin–streptomycin, glutamax, N2, EGF, FGF2, insulin, Y27632 (10 μM; Abcam, cat#ab120129), 10 % R-spondin1–conditioned medium, and 50 % Wnt3a-conditioned medium] was added to each well.

One week after seeding, gels were dissolved using Dispase enzyme (1 mg/ml in DMEM/F12 at 37 °C for 30 min). The released organoids were first counted and then dissociated into single cells using 0.05 % trypsin-EDTA. The cells were reseeded in BME to start a new passage and kept in culture for seven days to assess self-renewal potential.

Organoid irradiation and drug treatments

Organoids at day 5 in culture were irradiated with 7 Gy photons using a Cesium-137 source with a dose rate of 0.59 Gy/min.

Mdivi-1 treatment (10 μM, MedChemExpress, cat#HY-15886) or equivalent volume of solvent (DMSO) for controls were performed in 5 and 8 day-old organoids.

MFI8 treatment (20 μM, MedChemExpress, cat#HY-150031) or equivalent volume of solvent (DMSO) for controls were performed at 3 days after irradiation.

UA treatment (1 μM, MedChemExpress, cat#HY-100599) or equivalent volume of solvent (DMSO) for controls were performed at 3 and 5 days after irradiation.

PMI treatment (10 μM, MedChemExpress, cat#HY-115576) or equivalent volume of solvent (DMSO) for controls were performed at 3 and 5 days after irradiation.

Caspase 3/7 assay

Irradiated and non-irradiated (control) salivary gland organoids were collected and immediately treated with CellEvent™ Caspase-3/7 Detection Reagent (cat#C10423, Thermo Fischer Scientific). Green fluorescence intensity was measured in whole wells after 16 h of incubation post-irradiation using an IncuCyte S3 microscope (Essen Bioscience) under 10X magnification and 300 ms exposure. The average Green Fluorescent Intensity per Object was calculated for each sample. For outlier exclusion an upper fluorescence threshold was calculated based on the mean fluorescent intensity across technical replicates ($\mu + 1.5\,\sigma$). Caspase-3/7 activity was next calculated relative to control samples.

Flow cytometry

For the measurement of the mitochondrial membrane potential and total mitochondrial mass, the probes TMRE (MedChemExpress, cat#HY-D0985A) and Mitotracker Green (ThermoFisher Scientific, cat#M7514) were used at a final concentration of 200 nM. For the measurement of intracellular ROS the probe H2DCFDA (MedChemExpress, cat#HY-D0940) was used at a final concentration of 5 μM. In brief, salivary gland organoids were collected, dissociated into single cells and resuspended with fresh culture medium. The desired probe was added to the cell suspension and incubated at 37 °C for 30 min. Cells were then spun down (for 5 min at 400 g) and washed with PBS/BSA 0.2 %. Cells were resuspended in PBS/BSA 0.2 % and analyzed using the NovoCyte Quanteon flow cytometer. Data was analyzed using the FlowJo software.

For the cell cycle analysis, mouse salivary gland organoids were harvested and trypsinized into single cells. Single cells were next washed with DPBS and fixed with 4 % PFA for 10 min. Fixed cells were permeabilized using 70 % (v/v) ice cold ethanol for 30 min and washed twice with DPBS prior to nucleic acid staining with working buffer (DAPI 2 μg/mL, RNAse 50 μg/mL, Triton X-100 0.1 %). Cell cycle was analyzed under a Watson (Pragmatic model) using the NovoExpress Flow Cytometry Software in a NovoCyte Quanteon flow cytometer instrument (Agilent Technologies, Inc, CA, USA).

Quantitative real-time PCR

Total RNA was extracted from organoids by using RNeasy Mini Kit (Qiagen, cat#74104) according to the manufacturer's instructions. Reverse transcription to cDNA was performed by using 1 μL dNTP mix (10 mM, cat# 10297–018), 1 μL random primers (100 ng, cat#SO142), 4 μL 5x First-strand Buffer (cat#28025013), 2 μL DTT (0.1 M, cat328025013), 1 μL RNase OUTTM (40 units/μL, cat#10777019), and 1 μL M−MLV RT (200 units, cat#28025013), reagents were purchased from Invitrogen. To measure the expression of the genes of interest, specific primers were used together with iQ SYBR Green Supermix (Bio-Rad, cat# 170–8885). The list of primers is specified in Supp. Table 1. The *Ywhaz* gene was used as internal control.

Mitochondrial DNA content

For the determination of mitochondrial DNA copy number, genomic DNA was extracted from organoids by using Monarch Genomic DNA purification Kit (New England Biolabs, cat#T3010S) according to the manufacturer's instructions. Genomic DNA was amplified using specific primers for mitochondrial DNA or nuclear DNA. The list of primers is specified in Supp. Table 1. *Ywhaz* and *Tert* were used as a reference for nuclear DNA.

Western blot

Organoids were collected and lysed with RIPA buffer. The lysates were sonicated and spun down at 4 °C (for 5 min at max speed). The protein concentration of the lysates was measured using the Bradford quantification method. Before loading, the samples were boiled at 99 °C for 5 min and an equal amount of protein was separated with 10 or 12 % polyacrylamide gels. The transfer to nitrocellulose membranes was performed using the Trans-Blot Turbo System (Bio-Rad). After blocking with 10 % milk in PBS-Tween20 for 30 min, membranes were cut and incubated with primary antibodies at 4 °C overnight followed by incubation with horseradish peroxidase-conjugated secondary antibodies at room temperature for 1.5 h. Membranes were developed using ECL reagent (Thermo Fisher Scientific, cat#32106) in a ChemiDoc imager (Bio-Rad). Western blots analysis was performed using Image Lab software. The list of primary antibodies is specified in Supp. Table 2.

SA-β-Galactosidase staining

Organoids were harvested at day 11, fixed and stained for 4 h with X-Gal solution (pH 6) according to the manufacturer's instructions (Merck Millipore, cat#KAA002RF). Organoids were imaged using a Leica DM6 microscope and blue-stained cells were considered as senescent cells.

The quantification of the SA-β-Gal staining of control and irradiated organoids, DMSO/Mdivi-1-treated organoids and DMSO/MFI8-treated organoids has been performed using ImageJ, calculating the ratio between the blue area (positive area) and total area of the organoids.

For the quantification of the SA-β-Gal of DMSO/UA and DMSO/PMI-treated samples, organoids were harvested, fixed and incubated for 30 min in Bafilomycin A1, followed by SPiDER-β-Gal reagent as indicated by the manufacturer's instructions (Dojindo EU GmbH, Munich Germany). The samples were next stained with propidium iodide (1 μg/mL) in PBS-Triton X-100 (0.4 %). Samples were imaged using an IncuCyte® S3 microscope (Essen BioScience). The Green fluorescent intensity (300 ms) and red fluorescent intensity (600 ms) of whole-well scans were measured and the green / red area ratio was used for normalization.

Immunofluorescence staining

For staining of the mitochondrial network, salivary gland organoids were harvested at day 11 and dissociated into single cells. Cells were counted and 90.000 cells were re-seeded on the top of a coverslip in a 24 well plate. WRY media was added and cells were incubated at 37 °C overnight. On the next day cells were fixed with 4 % formaldehyde and incubated with the primary antibody at 4 °C overnight. Cells were then incubated with the secondary antibody at room temperature for 1 h. DAPI (Sigma Aldrich, cat#D9542) was used for nuclear staining.

For the staining of DRP1 and PINK1, previously archived mouse salivary gland tissue sections were used. In brief, tissue sections were first dewaxed and then incubated with the proper primary antibody at 4 °C overnight. On the next day, sections were incubated with the secondary antibody for 1 h at room temperature and DAPI for 10 min at room temperature.

All images were acquired with a Leica DM6 microscope and quantified using ImageJ. The list of antibodies is specified in Supp. Table 2.

Statistical analysis

Statistical analyses were performed using the GraphPad Software version 8. Two-tailed Student's *t*-test and two-way ANOVA were used to determine significant differences between groups. All values are represented as mean ± s.e.m. In all experiments, replicates were samples derived from different animals, the number of biological replicates (n) used in each experiment is stated in the figure legend. p-values ≤ 0.05 were considered statistically significant.

Results

To evaluate the effect of radiation on the close interconnection between mitochondrial function and cellular senescence, we used our previously established mSGO model. Consistent with the findings of Peng et al. [20], we applied a dose of 7 Gy, which was shown to induce a significant increase in senescent markers. Thus, mSGOs were irradiated with 7 Gy photons and analyzed 6 days later (day 11) (Fig. 1A). After irradiation, mSGOs displayed low levels of apoptosis at both 16 h and 6 days post-irradiation (Supp. Fig. 1A). However, they exhibited a significant cell cycle arrest (Supp. Fig. 1B) and increased levels of senescence-associated-β-Galactosidase (SA-β-Gal) at 6 days post-irradiation (Fig. 1B), indicating an accumulation of senescent cells in the irradiated samples. Moreover, qPCR and western blot analyses showed increased levels of the cell cycle regulator P21 (*Cdkn1a*) and SASP factors following irradiation (Fig. 1C-E), confirming our previously published data [20].

To evaluate the state of mitochondria after irradiation, we assessed different mitochondrial parameters, including mitochondrial mass, mitochondrial membrane potential (ΔΨM) and mitochondrial DNA (mtDNA) copy number. Flow cytometry analysis showed a significant increase in the total mitochondrial mass after irradiation, as measured by the mean intensity of Mitotracker Green (Fig. 1F), and in agreement with the fact that senescent cells are often characterized by an increased number of mitochondria [12]. Alongside this response, we observed a significant decrease in ΔΨM (Fig. 1G), suggesting an accumulation of non-functional mitochondria. An increase in malfunctioning mitochondria has been associated with increased ROS production, which can further damage the cell [21]. Indeed, flow cytometry analysis showed a significant increase in H2DCFDA mean intensity after irradiation, which indicates enhanced ROS generation in irradiated organoids compared to control (Fig. 1H). Additionally, gene expression via qPCR analysis revealed a significant decrease in the total amount of mtDNA after irradiation (measured as mtDNA copy number, Fig. 1I). A lower amount of mtDNA has previously been shown to be involved in aging and diseases [22–24]. This data confirms that radiation induces senescence and an accumulation of dysfunctional mitochondria.

Mitochondrial dynamic processes are essential for maintaining mitochondrial bioenergetics and function [25]. However, to date, little is known about the potential effects of radiation on mitochondrial dynamics in the context of normal tissue stem/progenitor cells. In line with previous studies [26], irradiation led to upregulation of mitochondrial

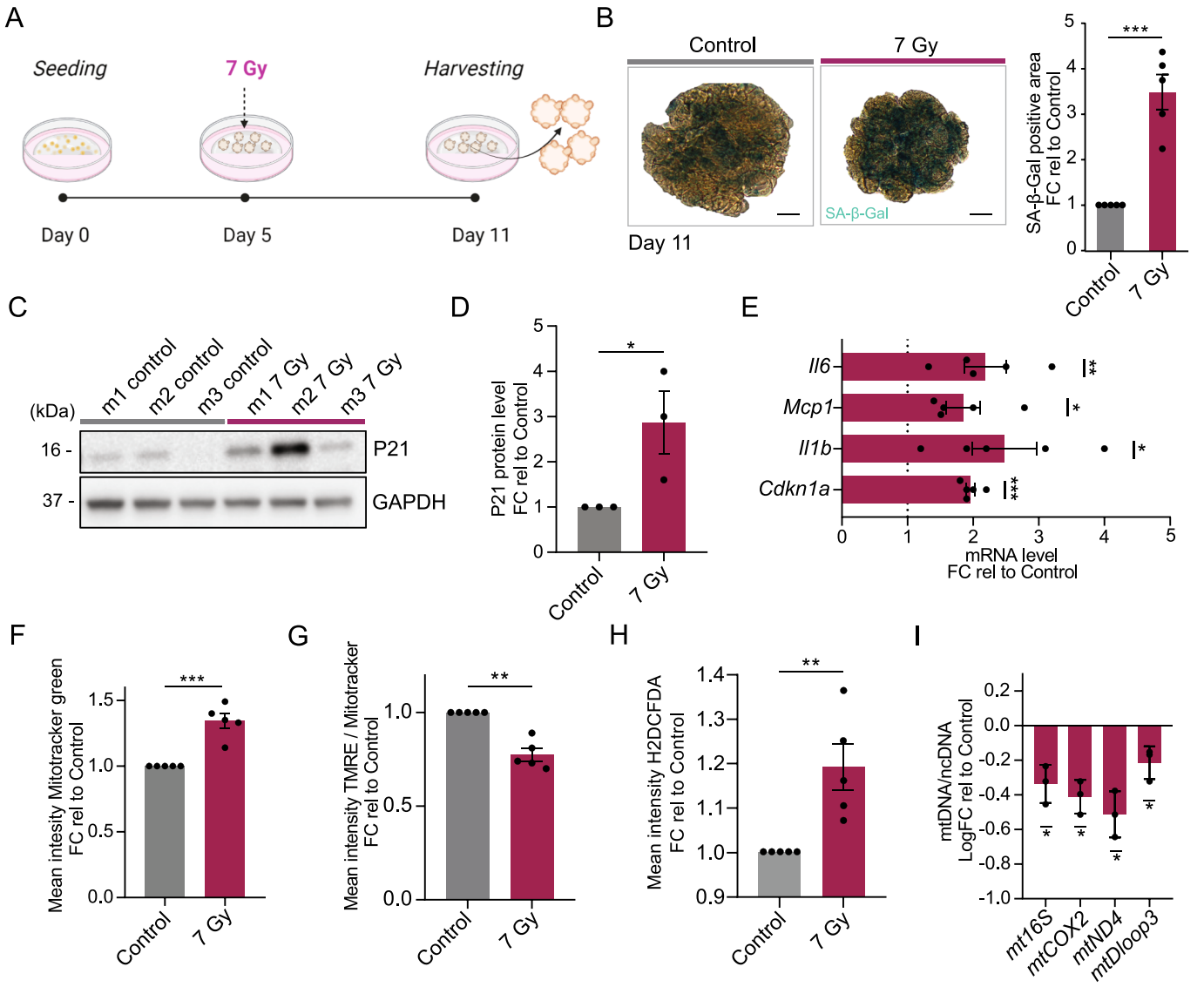

Fig. 1. Radiation-induced senescence and mitochondrial dysfunction. A. Experimental timeline, salivary gland organoids were irradiated at day 5 and collected at day 11 for the analysis. **B.** Representative images of whole mount SA-β-Gal staining in non-irradiated (control) and irradiated (7 Gy) salivary gland organoids (left), and SA-β-Gal quantification (right) (n = 5 animals/group). **C.** Western blot analysis of P21 in non-irradiated (control) and irradiated (7 Gy) salivary gland organoids (analysis performed on samples derived from 3 different animals, m1 – m3). **D.** P21 western blot quantification, data was normalized to GAPDH (n = 3 animals/group). **E.** rt-qPCR analysis of senescence-related genes (n = 5 animals/group). **F.** Flow cytometry analysis of total mitochondrial mass measured as mean intensity of Mitotracker green (n = 5 animals/group). **G.** Flow cytometry analysis of mitochondrial membrane potential measured as mean intensity of TMRE normalized to Mitotracker green (n = 5 animals/group). **H.** Flow cytometry analysis of total ROS measured as mean intensity of H2DCFDA (n = 5 animals/group). **I.** rt-qPCR analysis of mitochondrial DNA genes normalized to nuclear DNA genes (n = 3 animals/group). Scale bars, 10 μm. Data are means ± s.e.m. Student's *t*-test. *p < 0.05, **p < 0.01, ***p < 0.005. (For interpretation of the references to colour in this figure legend, the reader is referred to the web version of this article.)

fission proteins 2 days after 7 Gy photon irradiation (day 7) (Supp. Fig. 1C). However, western blot analysis revealed a strong downregulation of the fission proteins DRP1 and MFF at day 6 after irradiation, while no significant changes were detected in the expression of fusion proteins, such as MFN2 and OPA1 (Fig. 2A, B and Supp. Fig. 1D). Moreover, consistent with the previous observations, we detected a significant increase in TOMM20, a mitochondrial receptor commonly used as a marker of total mitochondrial mass, in irradiated samples (Fig. 2A, B and Supp. Fig. 1D). Next, to assess the effect of loss of mitochondrial fission on mitochondrial morphology, we performed immunofluorescence staining for TOMM20. As shown in Fig. 2C and Supp. Fig. 1E, irradiated samples exhibited elongated mitochondria and a denser mitochondrial network, further corroborating the observed reduction in mitochondrial fission.

To evaluate the potential link between loss of mitochondrial fission and mitochondrial dynamics dysregulation with the observed increase in senescence following irradiation, we treated control mSGOs with the mitochondrial division inhibitor-1 (Mdivi-1). Non-irradiated mSGOs were treated with Mdivi-1 at 5 and 8 days after seeding, and samples were collected on day 11 for analysis (Supp. Fig. 2A). Mdivi-1 and DMSO-treated samples exhibited a similar number of organoids, shown as organoid forming efficiency (OFE) (Supp. Fig. 2B, C). However, Mdivi-1 treatment slightly affected organoid growth, as demonstrated by the reduced total cell number (Supp. Fig. 2B, C). To assess the presence of senescence, we performed whole mount SA-β-Gal staining. As shown in Fig. 2D and Supp. Fig. 2D, inhibition of fission led to an increased number of senescent cells. Moreover, qPCR analysis showed a significant upregulation of some SASP factors following Mdivi-1 treatment (Fig. 2E). Next, to confirm the importance of mitochondrial fission loss in promoting senescence in irradiated samples, we enhanced

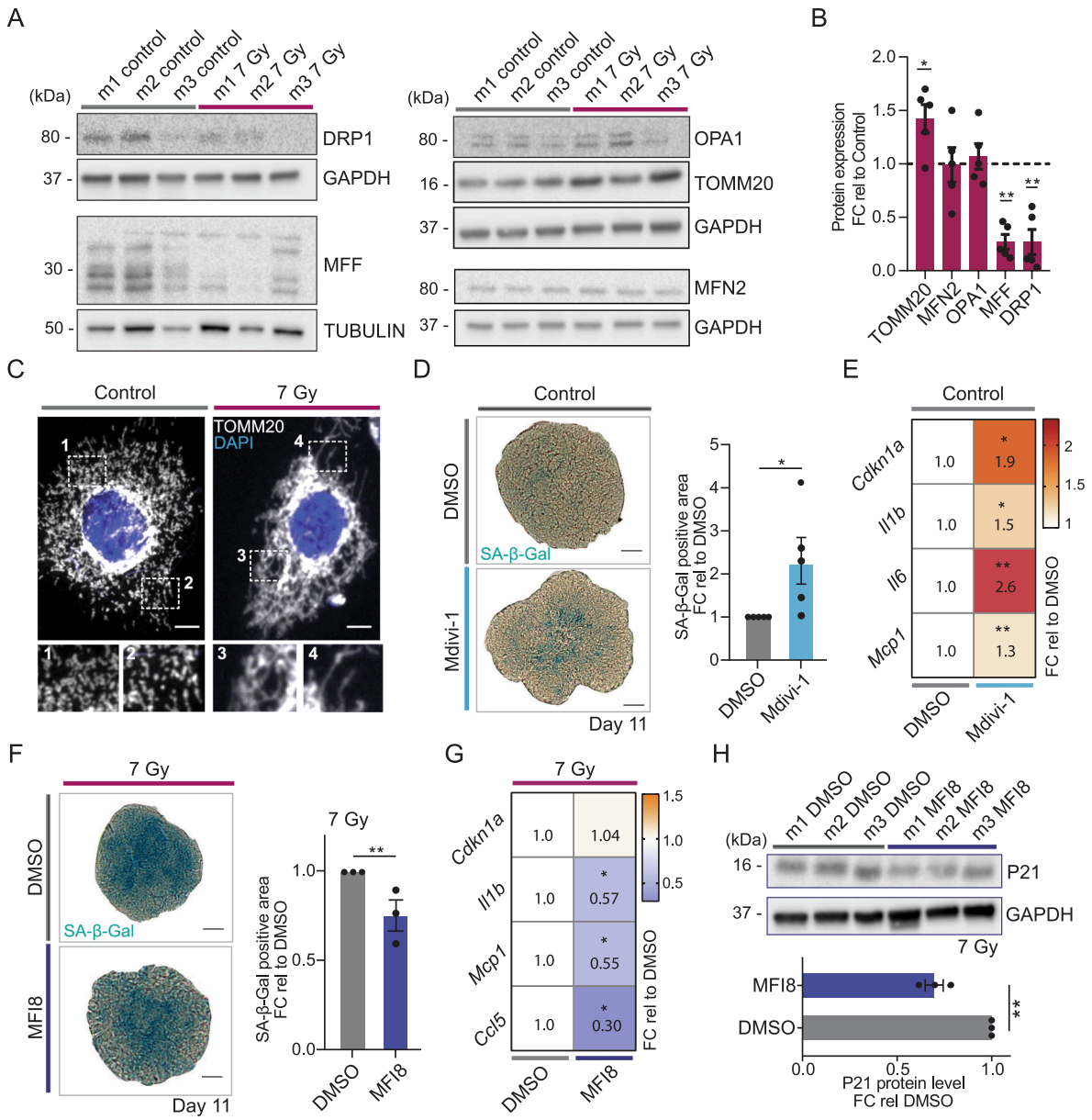

Fig. 2. Impaired mitochondrial dynamics after irradiation. A. Western blot analysis of fission-related proteins (left) and fusion-related proteins (right) in non-irradiated (control) and irradiated (7 Gy) salivary gland organoids (analysis performed on samples derived from 3 different animals, m1 – m3). **B.** Western blot quantification, data was normalized to GAPDH or TUBULIN. Western blot images for mouse 4 (m4) and mouse 5 (m5) are provided in Supp. Fig. 1A (n = 5 animals/group). **C.** Representative images of immunofluorescence staining of salivary gland cells, TOMM20 (white) and DAPI (blue). Boxes show zoom-ins of selected areas. Scale bar, 5 μm. **D.** Representative images of whole mount SA-β-Gal staining after DMSO and Mdivi-1 treatment in control salivary gland organoids (left). SA-β-Gal quantification (right). Scale bar, 10 μm. n = 5 animals/group. **E.** Heatmap showing the average gene expression of senescence-related genes detected by rt-qPCR after Mdivi-1 and DMSO treatment (n = 4 animals/group). **F.** Representative images of whole mount SA-β-Gal staining after MFI8 and DMSO treatment in irradiated (7 Gy) salivary gland organoids (left). SA-β-Gal quantification (right). Scale bar, 10 μm. n = 3 animals/group. **G.** Heatmap showing the average gene expression of senescence-related genes detected by rt-qPCR after MFI8 and DMSO treatment in irradiated (7 Gy) salivary gland organoids (n = 3 animals/group). **H.** Western blot analysis of P21 after DMSO and MFI8 treatment in irradiated (7 Gy) salivary gland organoids (analysis performed on samples derived from 3 different animals, m1 – m3) (top). P21 western blot quantification (bottom), data was normalized to GAPDH (n = 3 animals/group). Data are means ± s.e.m. Student's t-test and two-way ANOVA. *p < 0.05, **p < 0.01. (For interpretation of the references to colour in this figure legend, the reader is referred to the web version of this article.)

mitochondrial fission by treating irradiated mSGOs with the mitochondrial fusion inhibitor MFI8 [27] (Supp. Fig. 3A). Treatment with MFI8 led to a more pronounced mitochondrial network fragmentation compared to DMSO-treated samples (Supp. Fig. 3B). Notably, fission enhancement significantly decreased the levels of SA-β-Gal (Fig. 2F and Supp. Fig. 3C), SASP-related gene expression (Fig. 2G and Supp. Fig. 3D) and P21 protein (Fig. 2H and Supp. Fig. 3E) in irradiated samples. Moreover, MFI8 treatment improved mSGOs organoid growth as shown by the increase of total number of cells at day 11 (Supp. Fig. 3F). Taken together, this data confirms the involvement of dysregulated mitochondrial dynamics in enhancing cellular senescence in normal tissue-derived mSGOs. Indeed, our data indicate that loss of mitochondrial fission contributes to the accumulation of non-functional mitochondria and the increased senescence observed after irradiation.

The maintenance of mitochondrial homeostasis relies on a balanced mitochondrial dynamics and an efficient clearance of damaged mitochondria via mitophagy [28]. Therefore, we sought to determine whether the observed loss of mitochondrial fission and accumulation of

dysregulated mitochondria following irradiation were associated with reduced mitophagy. qPCR analysis revealed a significant down-regulation of mitophagy-related genes such as PTEN-induced putative kinase 1 (*Pink1*), Parkin RBR E3 Ubiquitin Protein Ligase (*Parkin2*), BCL2 Interacting Protein 3 (*Bnip3*) and BLC2 Interacting Protein 3 Like (*Bnip3l*), after irradiation (Fig. 3A). Moreover, western blot analysis showed a decrease of BNIP3 protein levels in irradiated samples (Supp. Fig. 4A, B), which has been shown to play a pivotal role in regulating mitophagy and mitochondrial function in different conditions [29]. Notably, in agreement with our *in vitro* findings, immunofluorescence staining of mouse salivary gland tissues showed reduced levels of the mitochondrial fission protein DRP1 and the mitophagy regulator PINK1 in the ductal compartments at 30 days after local salivary gland irradiation with 15 Gy X-rays (Supp. Fig. 2E). These results aligned with our previous study, where we observed an accumulation of senescent cells in striated and excretory ducts, which are believed to harbor salivary gland stem/progenitor cells [20,30].

Reduced mitophagy and the consequent loss of normal

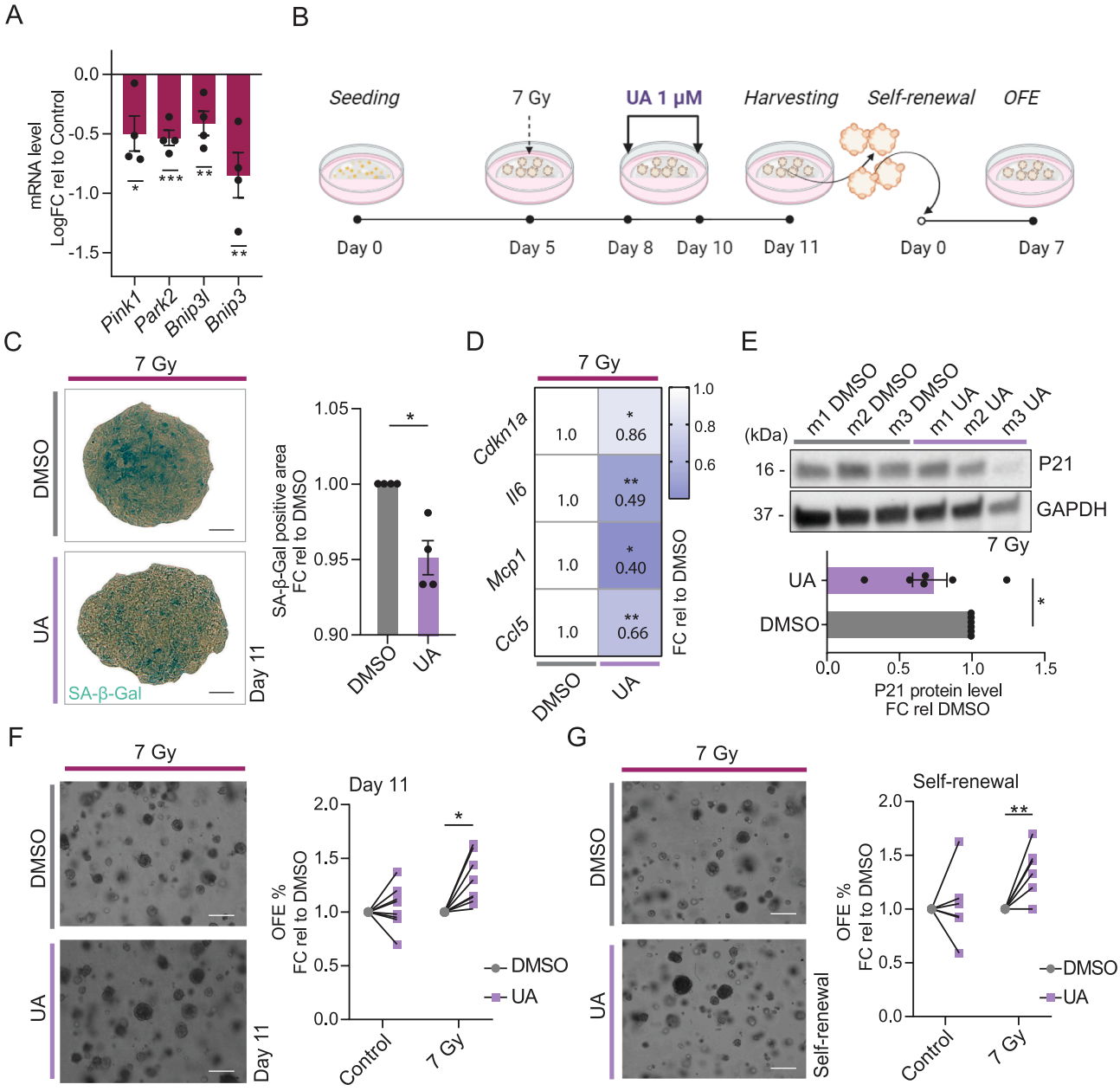

Fig. 3. Activation of mitophagy ameliorates salivary gland organoid growth and self-renewal capacity. A. rt-qPCR analysis of mitophagy-related genes (n = 4 animals/group). **B.** Experimental timeline, organoids were treated with UA (1 µM) at day 3 and 5 after irradiation. Samples were collected at day 11 and re-plated to assess self-renewal potential. **C.** Representative images of whole mount SA-β-Gal staining after DMSO and UA treatment in irradiated (7 Gy) salivary gland organoids (left). SA-β-Gal quantification (right). Scale bar, 10 µm. n = 4 animals/group. **D.** Heatmap showing the average gene expression of senescence-related genes detected by rt-qPCR after DMSO and UA treatment in irradiated (7 Gy) salivary gland organoids (n = 6 animals/group). **E.** Western blot analysis of P21 after DMSO and UA treatment in irradiated (7 Gy) salivary gland organoids (analysis performed on samples derived from 3 different animals, m1 – m3) (top). P21 western blot quantification (bottom), data was normalized to GAPDH. Western blot images for mouse 4 (m4), mouse 5 (m5) and mouse 6 (m6) are provided in Supp. Fig. 4F (n = 6 animals/group). **F.** Representative images of irradiated organoids in culture at day 11 after DMSO and UA treatment (left). Organoid quantification shown as percentage of organoid forming efficiency (OFE %) (right). Scale bar, 100 µm. n = 5 animals/group. Each irradiated sample was normalized to its own control. **G.** Representative images of organoids in culture after self-renewal (left). Organoid quantification shown as OFE % (right). Scale bar, 100 µm. n = 5 animals/group. Each irradiated sample was normalized to its own control. Data are means ± s.e.m. Two-way ANOVA. *p < 0.05, **p < 0.01.

mitochondrial turnover are strongly linked with mitochondria accumulation and the senescent phenotype [31]. We here treated organoids with UA, previously shown to increase mitophagy [32], or DMSO at 3 and 5 days after irradiation and assessed the expression of senescence markers, organoid growth and their ability to self-renew on day 11 (Fig. 3B). qPCR analysis showed an increased expression of mitophagy markers in UA-treated samples (Supp. Fig. 4C), accompanied by a decrease in senescent cells detected by whole mount SA-β-Gal staining (Fig. 3C and Supp. Fig. 4D). Furthermore, qPCR and western blot analysis exhibited a significant reduction of some SASP factors, such as *Il6*, *Mcp1* and *Ccl5* (Fig. 3D and Supp. Fig. 4E) and the cell cycle arrest marker P21 (*Cdkn1a*) (Fig. 3D, E and Supp. Fig. 4E, F) in irradiated samples, confirming the positive effect of UA in attenuating radiation-induced senescence in mSGOs. To further corroborate our findings with UA, we assessed senescence levels upon treatment of irradiated mSGOs with another mitophagy inducer. For this purpose, mSGOs were treated with the P62-mediated mitophagy inducer (PMI) [33] at days 3 and 5 after irradiation and analyzed on day 11 (Supp. Fig. 5A). Similar to UA, PMI treatment significantly reduced senescent markers (Supp. Fig. 5B-D), confirming the induction of mitophagy as an effective strategy to mitigate radiation-induced senescence.

Next, to assess the effect of UA on stem/progenitor cell activity and organoid growth, we first calculated the number of mature organoids at day 11 (shown as OFE) and performed a self-renewal assay by dissociating and re-plating the organoids. UA-treated irradiated organoids showed a higher OFE compared to DMSO-treated samples (Fig. 3F and Supp. Fig. 4G). Moreover, both UA and PMI-treated samples exhibited higher self-renewal potential (Fig. 3G and Supp. Fig. 4G, Supp. Fig. 5E), indicating improved stem cell function after mitophagy induction, similar to what we observed after treatment with senolytics [5]. These findings suggest that UA partially attenuates the senescent phenotype by improving mitophagy. Moreover, UA increased organoid formation and self-renewal potential, indicating its positive role in enhancing stem/progenitor cell function after irradiation.

Discussion

Salivary gland stem cell homeostasis is tightly regulated, and endogenous and exogenous stress factors, including radiation, can disrupt its balance, resulting in reduced regenerative capacity contributing to long-term organ dysfunction after radiotherapy [34]. Mitochondria have been shown to play a crucial role in maintaining stem cell function in different tissues, and their dysregulation has been implicated in several inflammatory and aging-related diseases [35]. In this study, we demonstrate that irradiated mSGOs exhibit an accumulation of dysfunctional mitochondria due to defective mitochondrial dynamics and mitophagy. Notably, we observed that activation of mitophagy resulted in reduced senescence induction, improving both organoid growth and stem/progenitor cell activity after irradiation.

Radiation can promote senescence in the salivary gland stem/progenitor cell niche, partly contributing to the decline in regenerative capacity and tissue functionality [5,6]. In line with the findings of Peng et al. [5], we observed an increase in senescent markers in mSGOs after 7 Gy photon irradiation accompanied by an accumulation of dysfunctional mitochondria. The interplay between cellular senescence and mitochondrial dysfunction is multifaceted. On the one hand, senescent cells often exhibit an increased mitochondrial mass as a compensatory mechanism to cellular stress [12,36]. On the other hand, dysfunctional mitochondria with reduced mitochondrial membrane potential can contribute to the development of cellular senescence through ROS production and altered bioenergetics [12]. In agreement with this intricate relationship, our study revealed a profound dysregulation of the mitochondrial dynamic process following irradiation. In particular, we found a strong downregulation of mitochondrial fission, essential for mitochondrial division [37]. This resulted in a denser mitochondrial network characterized by longer and more connected mitochondria. It has been previously demonstrated that senescent cells can exhibit elongated mitochondria, which lead to reduced energy demand and increased resistance to apoptosis [38]. Intriguingly, the increased mitochondrial mass detected after irradiation was associated with a decrease in mtDNA copy number. Irazoki et. al [14] have recently demonstrated that mitochondrial elongation can lead to mtDNA leakage into the cytoplasm of muscle cells. This can be recognized by cytoplasmic nucleic acid sensors and ultimately being degraded by nucleases [34,39]. Since the mitochondria of irradiated mSGOs exhibited an elongated phenotype, the leakage of mtDNA may explain the simultaneous increase of the mitochondria number and decrease of mtDNA at later timepoints. Moreover, due to its important role in regulating cell bioenergetics, impaired mitochondrial dynamics and lack of mtDNA integrity can also affect stem cell function and proliferation, ultimately leading to a decline in their regenerative potential [40,41].

Mitochondrial fission plays a crucial role in regulating mitophagy, essential for the turnover and removal of damaged mitochondria [42]. Studies have demonstrated that loss of mitochondrial fission can impair mitophagy and alter the regular degradation of mitochondria [43]. Here, we observed a reduction in mitophagy following irradiation, indicating a decline in the mitochondrial quality control mechanisms and the clearance of dysfunctional mitochondria. These findings align with previous works highlighting mitophagy's impairment in senescence and aging-related diseases [31,44]. Mitophagy defects and the accumulation of damaged mitochondria in stem cells have been shown to affect their self-renewal ability and regenerative potential [17]. Additionally, studies have revealed that lack of mitophagy can impact stem cell reprogramming and pluripotency *in vitro* [45]. In line with this, we found that induction of mitophagy attenuated senescence and improved salivary gland stem/progenitor cell function after irradiation, highlighting the importance of mitophagy in maintaining stem/progenitor cell function under stress conditions.

Overall, our findings suggest that activation of mitophagy could help to prevent the radiation-associated premature decline in salivary gland stem/progenitor cell function by improving mitochondrial function and reducing senescence.

Although previous works from our group have established that SGOs are enriched in stem/progenitor cells and closely resemble the original tissue architecture [18,46], our model presents limitations such as the absence of immune cells and systemic inflammation. The secretion of SASP, for instance, is essential for the recruitment of immune cells and removal of senescent cells in aged and damaged tissues [47]. Moreover, since UA has been shown to be a well-tolerated orally available mitophagy inducer able to modulate inflammation and immunity in different contexts [32,48–50], *in vivo* experiments are required to comprehensively understand the effects of UA on radiation-induced mitochondrial dysfunction, senescence and immunity. In this way, therapeutic strategies aimed at enhancing mitophagy, or more broadly mitochondrial function, could be used as a potential treatment option to restore the regenerative capacity of salivary glands and thus mitigate the side effects of radiotherapy in HNC patients.

CRediT authorship contribution statement

Davide Cinat: Conceptualization, Methodology, Investigation, Visualization, Writing – original draft, Project administration. **Anna Lena De Souza:** Investigation. **Abel Soto-Gamez:** Investigation. **Anne L. Jellema-de Bruin:** Investigation. **Rob P. Coppes:** Supervision, Writing – review & editing, Funding acquisition. **Lara Barazzuol:** Supervision, Conceptualization, Writing – original draft, Writing – review & editing.

Declaration of competing interest

The authors declare that they have no known competing financial interests or personal relationships that could have appeared to influence

the work reported in this paper.

Acknowledgments

The Mitotracker green probe was kindly provided by Prof Dr A.M. Dolga (Department of Molecular Pharmacology, Faculty of Science and Engineering, Groningen Research Institute of Pharmacy (GRIP), University of Groningen, Groningen, The Netherlands). The MFN2 antibody was kindly provided by Dr M. Mauthe (Department of Biomedical Sciences of Cells & Systems, University Medical Center Groningen, Groningen, The Netherlands). The PINK1 antibody was kindly provided by Prof Dr Sven van IJzendoorn (Department of Biomedical Sciences of Cells & Systems, University Medical Center Groningen, Groningen, The Netherlands). Illustrations were created with BioRender.com.

This work was supported by the Dutch Cancer Society KWF Grant nrs: 12092 and 12458.

Appendix A. Supplementary material

Supplementary data to this article can be found online at https://doi.org/10.1016/j.radonc.2023.110028.

References

[1] Mody MD, Rocco JW, Yom SS, Haddad RI, Saba NF. Head and neck cancer. Lancet 2021;398:2289–99. https://doi.org/10.1016/S0140-6736(21)01550-6.
[2] Voshart DC, Wiedemann J, van Luijk P, Barazzuol L. Regional responses in radiation-induced normal tissue damage. Cancers 2021;13:367. https://doi.org/10.3390/CANCERS13030367.
[3] Vissink A, Mitchell JB, Baum BJ, Limesand KH, Jensen SB, Fox PC, et al. Clinical management of salivary gland hypofunction and xerostomia in head-and-neck cancer patients: successes and barriers. Int J Radiat Oncol 2010;78:983–91. https://doi.org/10.1016/J.IJROBP.2010.06.052.
[4] Kim JH, Brown SL, Gordon MN. Radiation-induced senescence: therapeutic opportunities. Radiat Oncol 2023;18:1–11. https://doi.org/10.1186/S13014-022-02184-2/FIGURES/3.
[5] Peng X, Wu Y, Brouwer U, van Vliet T, Wang B, Demaria M, et al. Cellular senescence contributes to radiation-induced hyposalivation by affecting the stem/progenitor cell niche. Cell Death Dis 2020;11:1–11. https://doi.org/10.1038/s41419-020-03074-9.
[6] Marmary Y, Adar R, Gaska S, Wygoda A, Maly A, Cohen J, et al. Radiation-induced loss of salivary gland function is driven by cellular senescence and prevented by IL6 modulation. Cancer Res 2016;76:1170–80. https://doi.org/10.1158/0008-5472.CAN-15-1671.
[7] Hernandez-Segura A, Nehme J, Demaria M. Hallmarks of cellular senescence. Trends Cell Biol 2018;28:436–53. https://doi.org/10.1016/j.tcb.2018.02.001.
[8] Miwa S, Kashyap S, Chini E, von Zglinicki T. Mitochondrial dysfunction in cell senescence and aging. J Clin Invest 2022;132:1–9. https://doi.org/10.1172/JCI158447.
[9] Li N, Ye Y, Wu Y, Li L, Hu J, Luo D, et al. Alterations in histology of the aging salivary gland and correlation with the glandular inflammatory microenvironment. IScience 2023;26:106571. https://doi.org/10.1016/j.isci.2023.106571.
[10] Li N, Li Y, Hu J, Wu Y, Yang J, Fan H, et al. A link between mitochondrial dysfunction and the immune microenvironment of salivary glands in primary Sjogren's syndrome. Front Immunol 2022;13:845209. https://doi.org/10.3389/FIMMU.2022.845209/BIBTEX.
[11] Cervantes-Silva MP, Cox SL, Curtis AM. Alterations in mitochondrial morphology as a key driver of immunity and host defence. EMBO Rep 2021;22:e53086. https://doi.org/10.15252/EMBR.202153086.
[12] Miwa S, Kashyap S, Chini E, von Zglinicki T. Mitochondrial dysfunction in cell senescence and aging. J Clin Invest 2022:132. https://doi.org/10.1172/JCI158447.
[13] Zamponi N, Zamponi E, Cannas SA, Billoni OV, Helguera PR, Chialvo DR. Mitochondrial network complexity emerges from fission/fusion dynamics. Sci Rep 2018;8:1–10. https://doi.org/10.1038/s41598-017-18351-5.
[14] Irazoki A, Gordaliza-Alaguero I, Frank E, Giakoumakis NN, Seco J, Palacín M, et al. Disruption of mitochondrial dynamics triggers muscle inflammation through interorganellar contacts and mitochondrial DNA mislocation. Nat Commun 2023:14. https://doi.org/10.1038/s41467-022-35732-1.
[15] Wan Y, Finkel T. The mitochondria regulation of stem cell aging. Mech Ageing Dev 2020;191:111334. https://doi.org/10.1016/J.MAD.2020.111334.
[16] Ma K, Chen G, Li W, Kepp O, Zhu Y, Chen Q. Mitophagy, mitochondrial homeostasis, and cell fate. Front Cell Dev Biol 2020;8:467. https://doi.org/10.3389/FCELL.2020.00467.
[17] Lin Q, Chen J, Gu L, Dan X, Zhang C, Yang Y. New insights into mitophagy and stem cells. Stem Cell Res Ther 2021;12:1–14. https://doi.org/10.1186/S13287-021-02520-5/TABLES/1.
[18] Maimets M, Rocchi C, Bron R, Pringle S, Kuipers J, Giepmans BNG, et al. Stem cell reports ar ticle long-term in vitro expansion of salivary gland stem cells driven by Wnt. Signals 2016. https://doi.org/10.1016/j.stemcr.2015.11.009.
[19] Rocchi C, Cinat D, Martinez PS, Jellema-De Bruin AL, Baanstra M, Brouwer U, et al. The Hippo signaling pathway effector YAP promotes salivary gland regeneration after injury. Sci Signal 2021:14. https://doi.org/10.1126/scisignal.abk0599.
[20] Peng X, Wu Y, Brouwer U, van Vliet T, Wang B, Demaria M, et al. Cellular senescence contributes to radiation-induced hyposalivation by affecting the stem/progenitor cell niche. Cell Death Dis 2020;11:1–11. https://doi.org/10.1038/s41419-020-03074-9.
[21] Herranz N, Gil J. Mitochondria and senescence: new actors for an old play. EMBO J 2016;35:701–2. https://doi.org/10.15252/embj.201694025.
[22] Spano L, Etain B, Meyrel M, Hennion V, Gross G, Laplanche JL, et al. Telomere length and mitochondrial DNA copy number in bipolar disorder: identification of a subgroup of young individuals with accelerated cellular aging. Transl Psychiatry 2022;2022:12. https://doi.org/10.1038/s41398-022-01891-4.
[23] Pyle A, Anugrha H, Kurzawa-Akanbi M, Yarnall A, Burn D, Hudson G. Reduced mitochondrial DNA copy number is a biomarker of Parkinson's disease. Neurobiol Aging 2016;38:216.e7. https://doi.org/10.1016/J.NEUROBIOLAGING.2015.10.033.
[24] Zhang Z, Yang D, Zhou B, Luan Y, Yao Q, Liu Y, et al. Decrease of MtDNA copy number affects mitochondrial function and involves in the pathological consequences of ischaemic stroke. J Cell Mol Med 2022;26:4157. https://doi.org/10.1111/JCMM.17262.
[25] Westermann B. Bioenergetic role of mitochondrial fusion and fission. Biochim Biophys Acta - Bioenerg 2012;1817:1833–8. https://doi.org/10.1016/J.BBABIO.2012.02.033.
[26] Yamamori T, Ike S, Bo T, Sasagawa T, Sakai Y, Suzuki M, et al. Inhibition of the mitochondrial fission protein dynamin-related protein 1 (Drp1) impairs mitochondrial fission and mitotic catastrophe after x-irradiation. Mol Biol Cell 2015;26:4607–17. https://doi.org/10.1091/mbc.E15-03-0181.
[27] Zacharioudakis E, Agianian B, Kumar MVV, Biris N, Garner TP, Rabinovich-Nikitin I, et al. Modulating mitofusins to control mitochondrial function and signaling. Nat Commun 2022;13:1–20. https://doi.org/10.1038/s41467-022-31324-1.
[28] Twig G, Shirihai OS. The interplay between mitochondrial dynamics and mitophagy. Antioxidants Redox Signal 2011;14:1939–51. https://doi.org/10.1089/ars.2010.3779.
[29] Gao A, Jiang J, Xie F, Chen L. Bnip3 in mitophagy: Novel insights and potential therapeutic target for diseases of secondary mitochondrial dysfunction. Clin Chim Acta 2020;506:72–83. https://doi.org/10.1016/J.CCA.2020.02.024.
[30] Rocchi C, Barazzuol L, Coppes RP. The evolving definition of salivary gland stem cells. Npj Regen Med 2021;6:1–8. https://doi.org/10.1038/s41536-020-00115-x.
[31] Korolchuk VI, Miwa S, Carroll B, Von Zglinicki T. Mitochondria in cell senescence: is mitophagy the weakest link? EBioMedicine 2017. https://doi.org/10.1016/j.ebiom.2017.03.020.
[32] Andreux PA, Blanco-Bose W, Ryu D, Burdet F, Ibberson M, Aebischer P, et al. The mitophagy activator urolithin A is safe and induces a molecular signature of improved mitochondrial and cellular health in humans. Nat Metab 2019;1:595–603. https://doi.org/10.1038/s42255-019-0073-4.
[33] East DA, Fagiani F, Crosby J, Georgakopoulos ND, Bertrand H, Schaap M, et al. PMI: a ΔΨm independent pharmacological regulator of mitophagy. Chem Biol 2014;21:1585–96. https://doi.org/10.1016/j.chembiol.2014.09.019.
[34] Cinat D, Coppes RP, Barazzuol L. DNA damage-induced inflammatory microenvironment and adult stem cell response. Front Cell Dev Biol 2021;9:729136. https://doi.org/10.3389/FCELL.2021.729136/BIBTEX.
[35] Lisowski P, Kannan P, Mlody B, Prigione A. Mitochondria and the dynamic control of stem cell homeostasis n.d. https://doi.org/10.15252/embr.201745432.
[36] Vasileiou PVS, Evangelou K, Vlasis K, Fildisis G, Panayiotidis MI, Chronopoulos E, et al. cells Mitochondrial Homeostasis and Cellular Senescence n.d. https://doi.org/10.3390/cells8070686.
[37] Tilokani L, Nagashima S, Paupe V, Prudent J. Mitochondrial dynamics: overview of molecular mechanisms. Essays Biochem 2018;62:341. https://doi.org/10.1042/EBC20170104.
[38] Mai S, Klinkenberg M, Auburger G, Bereiter-Hahn J, Jendrach M. Decreased expression of Drp1 and Fis1 mediates mitochondrial elongation in senescent cells and enhances resistance to oxidative stress through PINK1. J Cell Sci 2010;123:917–26. https://doi.org/10.1242/jcs.059246.
[39] Santa P, Garreau A, Serpas L, Ferriere A, Blanco P, Soni C, et al. The role of nucleases and nucleic acid editing enzymes in the regulation of self-nucleic acid sensing. Front Immunol 2021;12:1–25. https://doi.org/10.3389/fimmu.2021.629922.
[40] Hong X, Isern J, Campanario S, Perdiguero E, Ramírez-Pardo I, Segalés J, et al. Mitochondrial dynamics maintain muscle stem cell regenerative competence throughout adult life by regulating metabolism and mitophagy. Cell Stem Cell 2022;29:1298–1314.e10. https://doi.org/10.1016/J.STEM.2022.07.009.
[41] Ahlqvist KJ, Suomalainen A, Hämäläinen RH. Stem cells, mitochondria and aging. Biochim Biophys Acta - Bioenerg 2015;1847:1380–6. https://doi.org/10.1016/j.bbabio.2015.05.014.
[42] Wang X, Diwan A, Wang Z, Liang Q, Kobayashi S, Zhao F, et al. Mitochondrial fission and mitophagy coordinately restrict high glucose toxicity in cardiomyocytes. Front Physiol 2020;11:604069. https://doi.org/10.3389/fphys.2020.604069.
[43] Lee Y, Lee HY, Hanna RA, Gustafsson AB. Mitochondrial autophagy by bnip3 involves drp1-mediated mitochondrial fission and recruitment of parkin in cardiac

myocytes. Am J Physiol - Hear Circ Physiol 2011:301. https://doi.org/10.1152/ajpheart.00368.2011.
[44] Chen G, Kroemer G, Kepp O. Mitophagy: an emerging role in aging and age-associated diseases. Front Cell Dev Biol 2020;8:527573. https://doi.org/10.3389/FCELL.2020.00200/BIBTEX.
[45] Vazquez-Martin A, Van den Haute C, Cufí S, Corominas-Faja B, Cuyàs E, Lopez-Bonet E, et al. Mitophagy-driven mitochondrial rejuvenation regulates stem cell fate. Aging (Albany NY) 2016;8:1330–49. https://doi.org/10.18632/AGING.100976.
[46] Nanduri LSY, Baanstra M, Faber H, Rocchi C, Zwart E, De Haan G, et al. Purification and Ex vivo expansion of fully functional salivary gland stem cells. Stem Cell Rep 2014;3:957–64. https://doi.org/10.1016/j.stemcr.2014.09.015.
[47] Kale A, Sharma A, Stolzing A, Stolzing A, Desprez PY, Desprez PY, et al. Role of immune cells in the removal of deleterious senescent cells. Immun Ageing 2020;17:1–9. https://doi.org/10.1186/s12979-020-00187-9.
[48] Shen PX, Li X, Deng SY, Zhao L, Zhang YY, Deng X, et al. Urolithin A ameliorates experimental autoimmune encephalomyelitis by targeting aryl hydrocarbon receptor. EBioMedicine 2021;64:103227. https://doi.org/10.1016/j.ebiom.2021.103227.
[49] Toney AM, Fox D, Chaidez V, Ramer-Tait AE, Chung S. Immunomodulatory role of urolithin a on metabolic diseases. Biomedicines 2021;9:1–18. https://doi.org/10.3390/biomedicines9020192.
[50] Denk D, Petrocelli V, Conche C, Drachsler M, Ziegler PK, Braun A, et al. Expansion of T memory stem cells with superior anti-tumor immunity by Urolithin A-induced mitophagy. Immunity 2022;55:2059–2073.e8. https://doi.org/10.1016/j.immuni.2022.09.014.